

Power Hardware-in-the-Loop Verification of a Cold Load Pickup Scenario for a Bottom-up Black Start of an Inverter-dominated Microgrid

Mina Mirzadeh^{*,1)}, Robin Strunk¹⁾, Tobias Erckrath²⁾ and Axel Mertens¹⁾

1) Institute for Drive Systems and Power Electronics, Leibniz University Hannover
Welfengarten 1, 30163 Hannover, Germany

*Phone: +49 (0)511 762-2848

*Email: mina.mirzadeh@ial.uni-hannover.de

URL: www.ial.uni-hannover.de

2) Fraunhofer Institute for Energy Economics and Energy System Technology (IET)
Joseph-Beuys-Straße 8, 34117 Kassel, Germany

Acknowledgements

This work was supported by Federal Ministry for Economic Affairs and Climate Action on the basis of a decision by the German Bundestag. Project RuBICon, Funding number: 03EI4003A. The authors would like to acknowledge the technical support from OPAL-RT Germany GmbH for real-time simulations.

Keywords

«Smart microgrids», «Grid-forming converters», «Power Hardware-in-the-Loop», «Non-linear loads», «Demand response», «Smart meters», «Grid restoration»

Abstract

Black start capability is one of the challenges in the future grid, to be dominated by distributed power electronic converter systems. A bottom-up multi-master black start scenario based on droop-controlled grid-forming inverters was earlier introduced as a response to this challenge. With reduced reliance on the availability of smart loads, this paper adapts this scenario so that a minimum change in the current configuration of the low voltage residential load sector is required. Moreover, with a focus on the cold load pick-up response, the power-sharing among two grid-forming inverters in the presence of high inrush currents is investigated using Power Hardware-in-the-Loop tests and detailed load models. The results confirm the formation of a laboratory-scale islanded Microgrid through grid-forming inverters where smart meters coordinate an autonomous dynamic partial loading only based on local measurements.

1 Introduction

The conventional approach for a black start after a large-scale power outage is to restore the supply from the transmission grid with the help of bulk generation units [1]. With the increasing penetration of small distributed generation (DG) units, however, such concepts need to be adapted to allow for a bottom-up black start procedure in the distribution network when a fault has happened at higher voltage levels. Followed by a global power outage in a low voltage (LV) residential sector, small-scale inverter-based generation units could not only be responsible for the local demand but also a quick black start of an islanded Microgrid (MG).

On this track, a new concept was already introduced in [2] to enable the black start capability of DG in the LV grid with no dependency on the availability of communication channels. This concept counts on droop-based grid-forming (GFm) inverters and a demand-side participatory approach different from the typical remote central control schemes found in the literature. Similar to the droop behavior of

inverters, local measurement of voltage and frequency through smart meters is used as an indicator for the available power to allow a priority-based switching of individual smart household appliances. This scenario remains the base of this paper. However, in the transition towards the dominance of smart loads in the residential sector, this paper adapts the loading sequence for non-intelligent loads. Automated operation of circuit breakers for different rooms are used for demand-side management. In this way, each smart meter-controlled residential household turns into a self-switching unit contributing to a bottom-up black start.

Recent developments in addressing challenges in the integration of smart grid technologies have led to the creation of new validation methods based on real-time simulation (RTS) and Hardware-in-the-Loop (HIL) tests [3]. Correspondingly, this paper uses Power Hardware-in-the-Loop (PHIL) laboratory tests for the validation of the proposed restoration scheme. In these tests, a power amplifier emulates the load-side behavior through RTS while the DG units are represented with physical inverter systems.

As listed by [4], it is a challenge for the grid operators to test network restoration schemes under realistic conditions, especially feasible load characteristics. This is well in line with the findings in [5], which identify inadequate load models contributing to unsuccessful grid reconstruction. Therefore, it is important to count for appropriate representation of LV residential loads in black start studies. Counting for the laboratory limitation of hardware representation of LV residential loads, the analytical load models in [6] are used in this work to effectively reduce the gap between simulation and real-life recorded system responses. These component-level models are based on the startup current measurements of real household appliances and include their non-linearity and inrush behavior.

This paper is structured as follows: Section 2 provides the background description of the considered black start sequence (BSS) including the requirements in the operation of GFm inverters and residential loads. The PHIL setup is then specified in detail in Section 3 and the measurement results are shown in Section 4. Finally, the conclusion is drawn in Section 5.

2 Black Start Sequence

The BSS follows the specification in [2] for a blackout caused at a higher voltage level. The main objective in such a sequence is to initially build up an LV islanded Microgrid through the contribution of multiple DGs (multi-master approach). This MG will (partially) supply local loads and later will be able to resynchronize to the medium voltage (MV) level once it is restored. As shown in Fig. 1, the BSS is initiated by a leading GFm inverter, called *Master Seed*, that ramps up its output voltage to the nominal voltage V_N . Other GFm inverters in the MG, called *Master Fellows*, synchronize to this voltage, connect to the MG and take over a share of the required power. For simplicity, this paper considers a static assignment of the *Master Seed*. The next sections shortly provide the working principle of the supply-side, consisting of GFm inverters, and the requirements from the LV residential load-side based on a novel operation of smart meters (SM) and circuit breakers (CB).

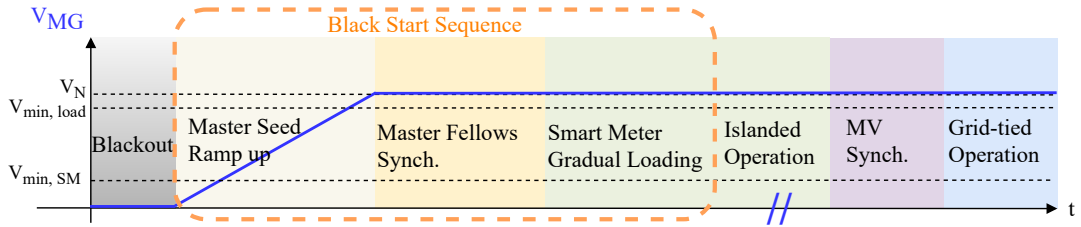


Fig. 1: Proposed BSS depicting the Microgrid voltage reference value (V_{MG}) with respect to the minimum required voltages for the smart meter ($V_{min,SM}$) and controlled loading ($V_{min,loading}$).

2.1 Grid-forming Inverter Operation

The inverters that restore the grid voltage after a blackout need to be controlled in a grid-forming mode as opposed to the grid-feeding mode, where the objective is only to deliver power without controlling the

voltage [7]. Here, inverters with a constant DC-link voltage and fixed available power are considered. This is a valid approximation of a battery storage system if only a short period is considered. Generally, inverters equipped with considerable energy storage are preferred for *Master* operation. Alternatively, inverters with fluctuating available power, e.g. PV-coupled systems, can also be controlled in a grid-forming mode. However, they need to curtail their output power during normal operation to enable flexible reactions to any load changes [8].

In the scope of this paper, a standard droop control with two cascaded inner control loops $G_V(s)$ and $G_I(s)$, respectively for the output voltage and current, are applied to all inverters, according to the block diagram shown in Fig. 2 [9]. $G_{LP}(s)$ is a low pass filter with the corner frequency ω_{LP} that adds virtual inertia to the droop control. G_V and G_I are both proportional-resonant (PR) controllers in the $\alpha\beta$ -frame, as indicated by the indices of the input and output quantities. The resonance frequency is always adjusted to match the reference frequency ω^* that is determined by the droop control. The transfer functions are

$$G_{LP}(s) = \frac{\omega_{LP}}{\omega_{LP} + s} \quad (1) \quad G_V(s) = K_{p,V} + K_{r,V} \frac{s}{s^2 + \omega^{*2}} \quad (2) \quad G_I(s) = K_{p,I} + K_{r,I} \frac{s}{s^2 + \omega^{*2}} \quad (3)$$

which are discretized according to the method proposed in [10]. Besides, a proportional controller $K_{p,I0}$ with a reference value of zero for the zero-sequence current is added in order to reduce the corresponding distortions in the laboratory setup. Furthermore, a feedforward path for the voltage reference, a virtual inductance L_v and an active damping resistance R_{ad} are included in the control. The control parameters are tuned in dependence of the parameters of the LC filter and the required control bandwidth, as listed in Table I. The reference values for active power P^* and reactive power Q^* are set to zero in the absence of a secondary control. The grid forming inverters are equipped with an LC filter, where $v_{C,\alpha\beta}$ is the voltage across the capacitor, $i_{L,\alpha\beta}$ is the current through the inductance, $i_{C,\alpha\beta}$ is the current in the capacitor and $i_{out,\alpha\beta}$ is the output current. The reference voltage for the pulse-width modulation (PWM) is $v_{PWM,\alpha\beta}^*$. The sinusoidal reference for the output capacitor voltage $v_{C,\alpha\beta}^*$ is calculated from the voltage reference amplitude \hat{V}^* and angle θ^* . The amplitude of the current reference vector $i_{L,\alpha\beta}^*$ is limited to the rated current. However, the protection from the transient overcurrents with shorter time constants than the dynamics of the current control require the blocking of PWM pulses. Since operation in current limiting generally causes disturbance in voltage control, this work avoids triggering the current limiting through load-side management.

The GFm inverters share the load according to their $P\text{-}\omega$ and $Q\text{-}V$ droop coefficients: $m_P = \frac{2\pi \cdot 1\text{Hz}}{S_N}$ and $m_Q = \frac{0.1V_N}{S_N}$, respectively, where S_N is the rated power of the inverter and V_N is the nominal grid voltage. The chosen droop parameters are a compromise between smaller transient power oscillations and a wider range of frequency and voltage for easier detection of thresholds. The reference values for active power P^* and reactive power Q^* are set to zero as a secondary control is not considered. The *Master Fellows* synchronize to the voltage provided by the *Master Seed* by using a phase-locked loop (PLL) before connection. A proportional controller with gain $K_{p,PLL}$ and a low-pass filter with corner frequency $\omega_{LP,PLL}$ are used in the PLL. At the time of connection, the voltage and frequency measured by the PLL are taken as initial reference values for the droop control. Consequently, the power provided by the *Master Fellows* will ideally be zero at first. Then, the reference values are gradually changed to the nominal voltage V_N and frequency ω_N . As a result, the master fellows take over an equal share of power according to the droop coefficients. Any existing grid-feeding inverters would reconnect to the grid once the voltage is reestablished according to [2]. However, they are not considered in the PHIL setup to keep the focus on the interaction between the Gfm inverters and the load-side.

2.2 Load-side Requirements

Although there is an accelerating trend for manufacturers towards smart household appliances, the residential load profile still dominantly consists of conventional loads with no overlaid or remote control. Apart from current protection schemes via conventional CBs inside households, it is the responsibility of the grid provider to assure power quality to the loads in the allowed range (According to VDE-AR-N 4100: $0.8V_N < V < 1.1V_N$ and $47.5\text{Hz} < f < 51.5\text{Hz}$). Consequently, in the case of a blackout, since

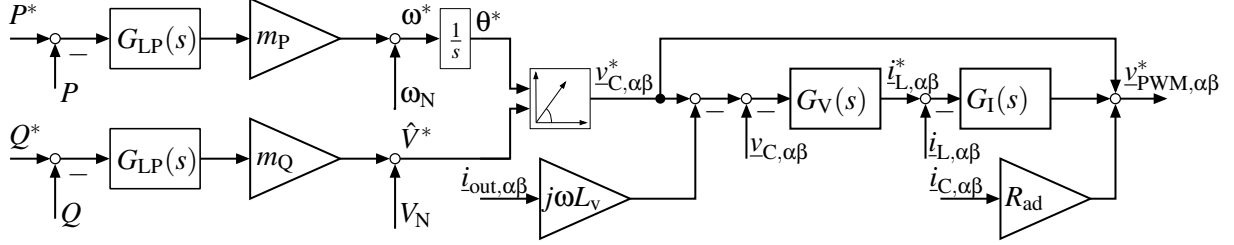


Fig. 2: Droop control with inner voltage and current control loops, virtual inductance and active damping for grid-forming inverters

Table I: Control parameters

Parameter	Symbol	Value
Corner frequency of the low-pass filter for the droop control	ω_{LP}	314 $\frac{\text{rad}}{\text{s}}$
$P-\omega$ droop coefficient	m_P	0.393 $\frac{\text{rad}}{\text{kW}\text{s}}$
$Q-V$ droop coefficient	m_Q	2.04 $\frac{\text{V}}{\text{kVAr}}$
Proportional gain of the voltage control	$K_{p,V}$	7.540 $\frac{\text{mA}}{\text{V}}$
Resonant gain of the voltage control	$K_{r,V}$	94.75 $\frac{\text{A}}{\text{Vs}}$
Proportional gain of the current control	$K_{p,I}$	2.67 $\frac{\text{V}}{\text{A}}$
Resonant gain of the current control	$K_{r,I}$	4195 $\frac{\text{Vs}}{\text{A}}$
Proportional gain of the zero-sequence current control	$K_{p,10}$	0.534 $\frac{\text{V}}{\text{A}}$
Virtual inductance	L_v	3 mH
Active damping resistance	R_{ad}	1 Ω
Proportional gain for PLL	$K_{p,PLL}$	266.7 $\frac{\text{rad}}{\text{s}}$
Corner frequency of the low-pass filter for the PLL	$\omega_{LP,PLL}$	158 $\frac{\text{rad}}{\text{s}}$

it is conventionally expected that only quality-assured power is restored from the MV level, the loads remain connected through the closed CBs and are then directly exposed to the BSS.

For a bottom-up black start, however, controllable loads are required to ensure the protection of loads and GFm units, and therefore increase the possibility of a successful black start. This is the case especially during the ramp-up by the *Master Seed* to avoid overloading, and later in the *Masters* Synchronization, where a low-load operation significantly reduces circulating transients among inverters. Until successful completion of *Masters* synchronization, the loads, on the other hand, should be protected from a grid, possibly far from its nominal operation values. Moreover, to increase the success of the black start even in low supply scenarios, a fair partial loading should be enabled at the household level. Consequently, smart units are required inside households to take care of switching on/off (*add/shed*) the loads.

2.2.1 Smart Meter-Controlled Circuit Breaker Operation

A demand-side response to black start capability is proposed in this paper with minimum implied requirements compared to the current residential configuration, as opposed to the device-level control proposed in [2]. As shown in Fig. 3 (right), a household is equipped with a smart meter that operates smart circuit breakers with normally-open operation, each assigned to one or two rooms, i.e load categories. The more smart circuit breakers configured to be controlled by the smart meter, the more distinctive the partial loading will be. The device-level switching in [2] can be therefore seen as the equivalent to the case where the number of CBs is equal to the number of loads. For a partial loading to be fair among different consumers, at least two smart circuit breakers are necessary per household. As a sample configuration, 3 smart circuit breakers are considered in Fig. 3, each controlling one phase. Assuming random assignment of phases to rooms in the LV grid, the gradual closure of the smart circuit breakers is not expected to introduce additional asymmetry to the overall system.

In the absence of external communication or a central control unit, the smart meter measures the input voltage magnitude and frequency and decides when each controllable circuit breaker should be opened

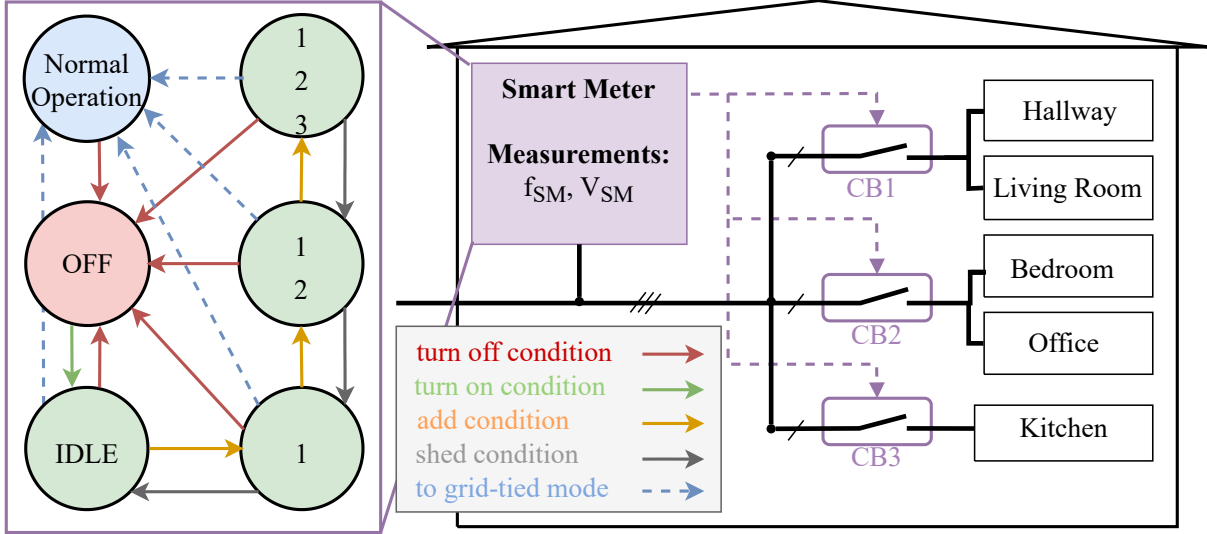


Fig. 3: Schematic of a representative household with a smart meter: sample configuration of 3 circuit breakers (right) and smart meter state machine during BSS (left)

or closed. Fig. 3 (left) shows a simplified state machine of the smart meter for 3 circuit breakers which can be further applied to more circuit breakers. The working principle is based on a *first in, last out* approach, where the highest priority is given to CB1, meaning it will be the first to be *added* and the last to be *shed*. Similarly, CB2 is given a higher priority than CB3. According to Fig. 3, the key conditions for smart meter state change can be defined as follows:

- The smart meter turns on once a minimum supply voltage $V_{\min,SM}$ is restored (turn on condition). It turns off at any point when voltage goes below this limit (turn off condition).
- The smart meter would only go back to its normal operation when a successful BSS ends (to grid-tied mode) through typical communications signals.
- The criterion to *add* or *shed* load categories is in line with the concept of under-frequency relays for non-critical loads in real MGs [11]. Generally, adding a load category follows an observation of a minimum voltage $V_{\min,\text{loading}}$ and a maximum frequency drop Δf (*add* condition). Furthermore, a category is *shed* when either the frequency drop exceeds Δf or the voltage drops below $V_{\min,\text{loading}}$ (*shed* condition).

Counting in for the droop behavior of GFm inverters, Δf should be predefined as $\Delta f = P_{\max,\text{load}} \cdot m_P$ where $P_{\max,\text{load}}$ is the maximum allowed loading in per unit active power. Therefore, according to the chosen value of m_P in this work, Δf should be kept smaller than 1 Hz. This ensures that loads are shed before the GFm inverters reach their current limit, counting for the reactive power demand in the grid and the transient power peaks due to inrush currents. A waiting time is considered between state changes to allow a stable frequency measurement and in the case of the first add, a successful synchronization of the *Masters*. Additionally, an internal flag is used to track the connection of each circuit breaker. This flag is used to avoid an immediate *add* followed by a *shed*. Table II shows the parameterization of the Smart Meter state machine, where the minimum voltage values for the smart meter and loading are chosen according to available smart meter data sheets and German grid codes, respectively. The maximum allowed loading $P_{\max,\text{load}}$, consequently defining the maximum allowed frequency drop, is the authors' choice for a conservative supply in the given testbench with the considered overcurrent protection. This marginal supply counts for the possible high-load transients between an *add* and a *shed*. Lastly, the waiting time is chosen based on the speed of the applied PLL and for better visibility in the RT tests.

Table II: Smart Meter State Machine Parameters

Parameter	Symbol	Value
Minimum supply voltage for the smart meter	$V_{\min,SM}$	80 V
Minimum supply voltage for loading	$V_{\min,loading}$	0.9 pu
Maximum allowed loading	$P_{\max,load}$	$\frac{2}{3}$ pu
Maximum frequency drop before <i>shed</i>	Δf	0.67 Hz
Waiting time between state change	T_{wait}	2 s

2.2.2 Residential Load Classification

This work considers a selection of balanced 3-phase loads representing typical residential loads in the Microgrid. Assuming a complementary assignment of phases to CBs, each appliance is considered as a symmetric three-phase device representing three identical single-phase devices in the Microgrid. A single smart meter is then sufficient to control all the controllable loads according to Fig. 3. Similar three-phase consideration is applied to the non-controllable loads, resulting in a significant reduction of computational burden for RTS.

As extensively discussed in [6], most residential household appliances show high levels of inrush currents when they startup, known in grid restoration literature as *cold load pickup*. For some Switch-Mode-Power-Supplies (SMPS) and Electric Machines (EM), the inrush current exceeds ten times the steady-state rated current. The aggregation of these inrush currents at the time of the black start could consequently exceed the current limits of the supplying inverters. Although this shows the necessity of fast overcurrent protection for all GFm inverters, optimized distribution of the aggregated inrush currents in a simulated black start event in [6] was shown effective in not only reducing the peak current values but also the duration of overcurrent operation. In this approach, low-power high-inrush current loads of class SMPS are initially switched on, followed by EMs with mid-power and mid-inrush current levels, and lastly the high-power resistive loads. Generally, the mentioned principle, *SMPS-first resistive-last*, should be used to prioritize loads in a one-time configuration of the smart meter, based on the number of CBs and the profile of the connected loads. It can be assumed that apart from a few portable devices like a charger or a vacuum cleaner, most of the devices are stationary within a household and therefore have a fixed CB connected.

In this paper, the smart meter is configured for a selection of typical appliances listed in Table III as follows: The rooms with the highest inrush currents (SMPS loads) were assigned to CB1. CB2 controls the loads in the bedroom/office with medium levels of inrush current. Last but not least, the kitchen with mostly resistive loads is assigned to CB3. The non-controllable load is kept smaller than the controllable load to represent a high penetration of smart meters in the Microgrid.

3 Power Hardware-in-the-Loop Laboratory Setup

The verification of the BSS is carried out in a PHIL laboratory setup, as shown in Fig. 4. Two 3-phase inverter systems, one as *Master Seed* and one as *Master Fellow*, are considered with the GFm control explained in section 2.1. Through different lengths of LV lines, the two *Masters* are physically connected to a power amplifier that emulates the behavior of the load with the characteristics explained in section 2.2. According to the current-type ideal transformer model [12], the control loop of the power amplifier is closed as shown in Fig. 5. The physical measurement of the voltage at the terminal of the power amplifier is passed via *Power Amplifier Interface* to an ideal 3-phase controllable voltage source in the RTS *Model*. A low pass filter with a corner frequency of 500 Hz is added to the voltage measurements in the simulation to increase the stability of the PHIL setup [3]. The RTS current of the aggregated load model is then passed as the current setpoint to *Power Amplifier Interface*. Additionally, the RT control is enabled through a console that provides RT monitoring and data logging. More details on the hardware characteristics and the RTS environment are given in the following sections.

Table III: Residential load configuration and component-level characteristics including inrush current I_{inrush} , and steady-state current I_{ss} according to measurements in [6].

Section	Appliances	Type	$I_{\text{inrush}}(\text{peak A})$	$I_{\text{ss}}(\text{peak A})$	$P_{\text{rated}}(\text{W})$
Controllable Loads: CB1 (Hallway/ Living room)	Vacuum Cleaner	EM	30.7	8.3	1400
	TV (stand-by)	SMPS	4.8	0.3	2
	Chiller	SMPS	31.7	0.2	2100
Controllable Loads: CB2 (Bedroom/ Office)	Vacuum Cleaner	EM	13.6	9.3	850
	Fan	EM	0.4	0.3	45
	Printer (stand-by)	SMPS	19.6	0.6	1850
Controllable Loads: CB3 (Kitchen)	Residual	R	NA	8.1	2640
	Fridge	EM	12.6	1	90
	Toaster	R	NA	5.3	900
	Microwave	SMPS	5.5	9.1	1150
Non-controllable Loads	Electric Kettle	R	NA	14.1	2400
	Rice Cooker	R	NA	2.5	350
	LED	SMPS	0.2	0.1	2.3

3.1 Hardware Parameters

The power lines in the setup are modeled by physical passive components. One line section has a resistance of $70.3 \text{ m}\Omega$ and an inductance of $79.29 \mu\text{H}$ and resembles a cable of 340m length and the type NAYY 4 · 150 mm². As shown in Fig. 4, the *Master Seed* inverter is connected to the busbar via one line section while the *Master Seed* is connected via three line sections. The two *Masters* share a common DC-link. The DC-link voltage is set to a constant value of 730V and it is controlled by an active front end. The switching frequency is $f_s = 16 \text{ kHz}$ and the rated power of each inverter is $S_N = 16 \text{ kVA}$. Furthermore, both inverters comprise an LC filter with the parameters $L_f = 850 \mu\text{H}$ and $C_f = 10 \mu\text{F}$. Corresponding to the rated power, the rated peak current of each phase is 33A.

The power amplifier has a rated power of $S_N = 100 \text{ kVA}$ and a switching frequency of $f_s = 125 \text{ kHz}$. The DC-link voltage is 770V and is controlled by an active front end. The details of the filter and control design of the power amplifier are not known. However, it shall be noted here that resonance interactions between the filter of the power amplifier and the LC filters of the *Master* inverters might occur. A set of control parameters that leads to acceptable damping of any high-frequency oscillations is chosen. Further information and a picture of the laboratory setup can also be found in [13].

3.2 Real-time Residential Load Emulation

The Opal RT real-time simulator OP5707 is used in this CPU-based setup with a sampling time of $t_s = 50 \mu\text{s}$ that corresponds to the expected transients in the system and the switching frequency of the power amplifier while maintaining an RT execution. The coupled RT Lab software implements the ARTEMiS solver add-on in SimPowerSystems (SPS) of Matlab Simulink. This solver has a higher order (order 5) than SPS (order 2) which aims for higher accuracy in RTS. Additionally, since ARTEMiS precomputes and discretizes the typical state-space matrices of SPS in advance, it significantly reduces the computational time so that the real-time limit is not crossed [14]. As the electrical system expands, the size of the state-space matrix exceeds, causing memory flows for the precomputation of ARTEMiS. To overcome this challenge, a system decoupling is achieved with the State Space Nodal (SSN) methods [15] which divides the electrical system into nodal groups specified by the user. Each group is then solved by a state-space method while the nodal method computes the interface between the groups through SSN Nodal Interface Blocks (SSN NIB). In this way, the total size of the state-space matrices in the memory can be significantly reduced. However, not every SPS block is compatible with SSN NIB. The SPS-based models of resistive and SMPS loads of [6] can be further used in ARTEMiS RTS connected to V-type (virtual voltage source) SSN NIB. The SPS Asynchronous Machines, on the other hand, should be replaced by SSN Induction Machines (SSN IM) connected to X-type (external group) SSN NIB.

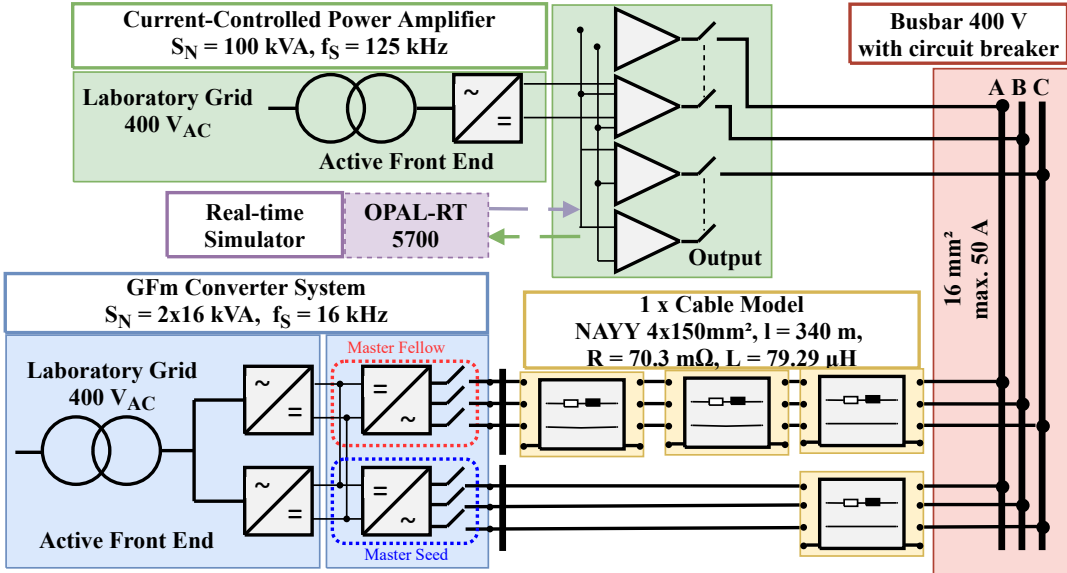


Fig. 4: System under test: MG consisting of GFm converters, a power amplifier, LV cable boxes, and an RTS considering an aggregated load model of multiple households in a symmetric operation.

The main challenge here is to intelligently introduce nodes to keep the system running in real-time. Generally, a minimum number of nodes should be introduced, while each group should be kept with a reasonable number of states and switches. The indicator of the size of the electrical system, i.e. the size of the corresponding state-space matrix, is the number of switches in each SSN group, the maximum of which is 15. For the residential configuration given in Table III, such optimization is carried out according to Fig. 5 as follows: Each EM with a 3-phase SSN IM model forms a nodal group through a separate 3-phase SSN NIB. For the SMPS load LED with 4 switches per phase, one nodal group is introduced for its 3-phase model (12 switches) through a 3-phase SSN NIB. It is important to note that since the current levels (both inrush and steady-state) of n number of LEDs are equal to n times the current levels of a single LED [16], the parameters of the circuit model of an LED are accordingly scaled to represent 20 instances with no additional switches needed in the circuit. In the case of the Microwave and the Printer, two additional breakers were used inside the SMPS model to count for the inrush behavior. Therefore, each phase of the device would unavoidably need a separate grouping (6 switches). Alternatively, for the TV and the Chiller in the same room, one 1-phase SSN NIB can mutually group each phase of the two SMPS loads (12 switches). Last but not least, the three 3-phase Circuit Breakers are grouped into a 3-phase SSN NIB (9 switches). In total, the residential load in this setup is grouped into 15 SSN nodes with moderate execution time and CPU usage, resulting in no overruns during operation. A resistor of $10\text{ m}\Omega$ per phase is assumed as the equivalent of the Smart Meter hardware. The voltage magnitude and frequency at the terminal of the Smart Meter are measured by a DSOGI-PLL, based on SPS blocks. The measurements are then fed to the Smart Meter state-machine which is implemented as a Moore-Machine in state-flow Simulink according to Fig. 3. The line model represents a service connection including the electricity meter and over-current protection elements with a standard length of 30 m and 6 m^2 cross-section ($R = 3.690 \frac{\Omega}{\text{km}}$, $X = 0.094 \frac{\Omega}{\text{km}}$), as specified in [17].

4 Measurement Results

All measurements results are based on the internal sensors of the power amplifier and the inverter systems. The PHIL demonstration of the proposed BSS is shown in Fig. 6. For a clear illustration of power-sharing between the GFm inverters, the harmonics are reduced via the application of a low pass filter with a corner frequency of 50 Hz to the active and reactive power measurements of the *Master Seed* and *Master Fellow* (P_{MS} , P_{MF} , Q_{MS} and Q_{MF} , respectively). The frequency f_{SM} and the voltage V_{SM} are measured with the PLL of the smart meter which is located at the load connection point in the RTS. The

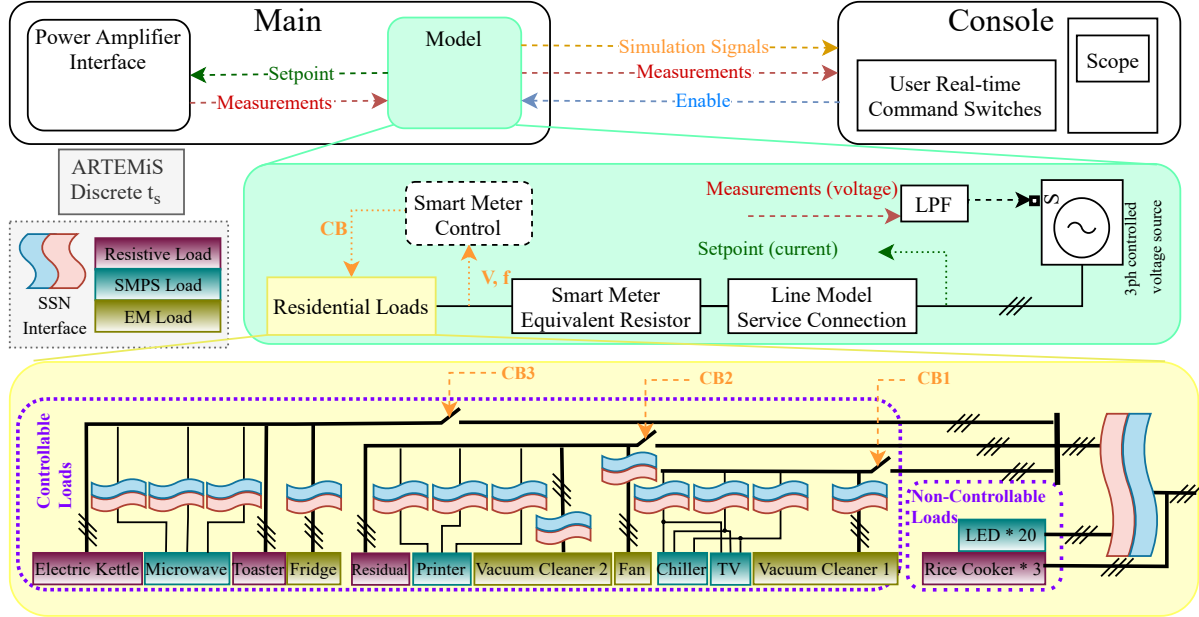


Fig. 5: Real-Time simulation environment and the optimized SSN grouping.

same PLL design as described in section 2.1 is also used for the smart meters.

The sequence starts with the voltage ramp up by the *Master Seed* that readily supplies the directly-connected base load as well as the significant demand of negative reactive power of the filter capacitor of the connected *Master Fellow*. The *Master Fellow* synchronizes to the sensed voltage and is enabled at $t = 6\text{ s}$, which leads to oscillations in the power. Due to the gradual change of the voltage and frequency setpoints of the *Master Fellow* to the nominal values, an equal active power-sharing of the two GFm inverters is achieved after approximately 3 s. At $t = 13\text{ s}$ the smart meter starts to add load categories according to its state machine. After category C is added, the frequency drops below the predefined threshold $\Delta f = 0.67\text{ Hz}$, corresponding to a power of $P_{\max,\text{load}} = \frac{2}{3}\text{ pu}$. Therefore, the smart meter sheds category C and the steady-state operation of the Microgrid is reached. While the frequency drop follows the active power of the GFm inverters according to the droop characteristic, the voltage drop not only depends on the reactive power but additionally on the virtual impedance in the control and the physical impedance of the power lines. Therefore, in the absence of an integral behavior in the Q-V droop and different lengths of the line of the two GFm inverters to the load, the reactive power is not equally shared.

In Fig. 7, the measured currents of the power amplifier i_{Load} are shown. The inrush currents at the connection of each load category are mainly caused by non-linear loads including diode rectifiers and induction machines. Since the inverters in this work are not equipped with a fast current limiting, the inrush currents become a bottleneck in the BSS. Although the inverters do not operate at nominal power in the steady-state, the peak current is already close to the maximum value of 33 A per inverter. Besides, the fast change of the current leads to high-frequency oscillations that are quickly damped. This can be explained by the interactions between the power amplifier and the inverter system and their respective filters. During steady-state operation with all load categories connected, the total harmonic distortion of the current is 2.7 %, well below the threshold 8 % specified by EN 61000-2-4.

5 Conclusion

In this paper, a bottom-up sequence is verified in Power Hardware-in-the-Loop laboratory tests to establish an islanded Microgrid after a blackout. The sequence requires a minimum hardware change of household circuit breakers but no external communication infrastructure. Following predefined rules, power is restored in the Microgrid based on a multi-master operation of droop-controlled inverters while the smart meters govern a partial loading. Cold load pickup is handled by smart meters through prioritized gradual adding of residential load groups according to their start-up behavior. On the other hand,

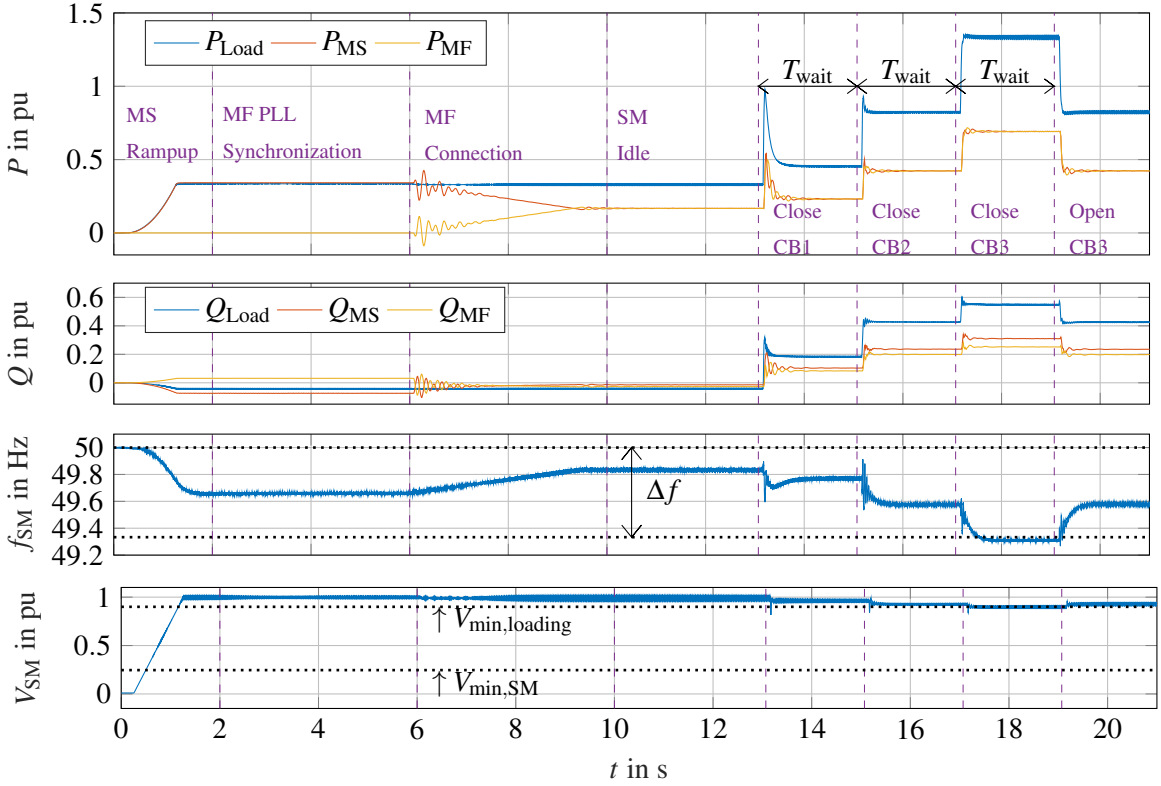


Fig. 6: PHIL measurements of the inverters and the SM during the proposed BSS. The base values of the per-unit system are the rated power S_N of each GFm inverter and the nominal grid voltage V_N .

an overload operation is reduced through the early shedding of the last added load groups. An aggregated household model comprising a variety of loads is successfully integrated into the test bench by real-time simulation. Withstanding peak inrush currents of the loads without triggering the protection of the grid-forming inverters is found as the bottleneck of the operation. Although such optimized distribution of load inrush currents minimizes the duration and level of overcurrent operation, further study into compatible fast current limiting methods is identified as a key requirement for higher reliability in the black start sequence and better protection of the grid-forming inverters. Furthermore, in case of moderate penetration of smart meters in the Microgrid, a lower voltage level and hence an earlier synchronization of grid-forming inverters should be further investigated to reduce the loading of the leading inverter that is responsible for the supply of uncontrollable base loads.

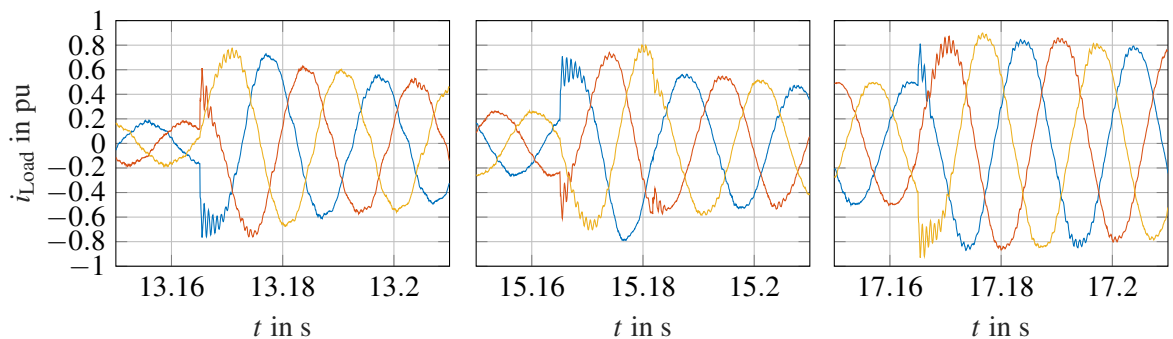


Fig. 7: Measured inrush currents at the connection time of CB1, CB2 and CB3. The base value of the per-unit system 1 pu = 66A peak is the accumulated rated current amplitude of both GFm inverters.

References

- [1] F. O. Resende, N. J. Gil, and J. A. P. Lopes, "Service restoration on distribution systems using Multi-MicroGrids," *Eur. Trans. Electr. Power*, vol. 21, no. 2, pp. 1327–1342, Mar. 2011, doi: 10.1002/etep.404.
- [2] M. Mirzadeh, et al, "A Rule-based Concept for a Bottom-up Multi-Master Black Start of an Inverter-Dominated Low-Voltage Cell," to be published in Proc. IEEE 13th International Symposium on Power Electronics for Distributed Generation Systems (PEDG), 2022.
- [3] J. Montoya et al., "Advanced Laboratory Testing Methods Using Real-Time Simulation and Hardware-in-the-Loop Techniques: A Survey of Smart Grid International Research Facility Network Activities," *Energies*, vol. 13, no. 12, Art. no. 12, Jan. 2020, doi: 10.3390/en13123267.
- [4] H. Haes Alhelou, M. Hamedani-Golshan, T. Njenda, and P. Siano, "A Survey on Power System Blackout and Cascading Events: Research Motivations and Challenges," *Energies*, vol. 12, no. 4, p. 682, Feb. 2019, doi: 10.3390/en12040682.
- [5] J. V. Milanovic, K. Yamashita, S. Martínez Villanueva, S. Ž. Djokic and L. M. Korunović, "International Industry Practice on Power System Load Modeling," in *IEEE Transactions on Power Systems*, vol. 28, no. 3, pp. 3038-3046, Aug. 2013, doi: 10.1109/TPWRS.2012.2231969.
- [6] M. Mirzadeh and A. Mertens, "Measurement-based Component-level Load Modeling for Evaluation of a Current-suppressing Loading Scenario for Microgrid Black Start Events," to be published in Proc. 13th IEEE PES ISGT North America 2022, Apr. 2022.
- [7] J. Rocabert, A. Luna, F. Blaabjerg and P. Rodríguez, "Control of Power Converters in AC Microgrids," in *IEEE Transactions on Power Electronics*, vol. 27, no. 11, pp. 4734-4749, Nov. 2012, doi: 10.1109/TPEL.2012.2199334.
- [8] M. E. Elkhatib, W. Du and R. H. Lasseter, "Evaluation of Inverter-based Grid Frequency Support using Frequency-Watt and Grid-Forming PV Inverters," 2018 IEEE Power & Energy Society General Meeting (PESGM), 2018, pp. 1-5, doi: 10.1109/PESGM.2018.8585958.
- [9] J. C. Vasquez, J. M. Guerrero, M. Savaghebi, J. Eloy-Garcia and R. Teodorescu, "Modeling, Analysis, and Design of Stationary-Reference-Frame Droop-Controlled Parallel Three-Phase Voltage Source Inverters," in *IEEE Transactions on Industrial Electronics*, vol. 60, no. 4, pp. 1271-1280, Apr. 2013, doi: 10.1109/TIE.2012.2194951.
- [10] S. A. Richter and R. W. De Doncker, "Digital proportional-resonant (PR) control with anti-windup applied to a voltage-source inverter," Proceedings of the 2011 14th European Conference on Power Electronics and Applications, 2011, pp. 1-10.
- [11] M. Barnes et al., "Real-World MicroGrids-An Overview," in 2007 IEEE International Conference on System-of Systems Engineering, Apr. 2007, pp. 1-8.
- [12] W. Ren, M. Steurer and T. L. Baldwin, "Improve the Stability and the Accuracy of Power Hardware-in-the-Loop Simulation by Selecting Appropriate Interface Algorithms," in *IEEE Transactions on Industry Applications*, vol. 44, no. 4, pp. 1286-1294, Jul-Aug. 2008, doi: 10.1109/TIA.2008.926240.
- [13] M. Dokus and A. Mertens, "On the Coupling of Power-Related and Inner Inverter Control Loops of Grid-Forming Converter Systems," in *IEEE Access*, vol. 9, pp. 16173-16192, 2021, doi: 10.1109/ACCESS.2021.3053060.
- [14] RT-LAB Help, ARTEMiS User's Guide, Version 2019.1.0.140, OPAL-RT Technologies.
- [15] C. Dufour, J. Mahseredjian and J. Belanger, "A combined state-space nodal method for the simulation of power system transients," 2011 IEEE Power and Energy Society General Meeting, 2011, pp. 1-1, doi: 10.1109/PES.2011.6038887.
- [16] J. F. G. Cobben and N. Arumdati, "Inrush Related Problems Caused by Lamps and Electric Vehicle," in Conference on Applied Electromagnetic Technology (AEMT), Lombok, Jul. 2011, p. 7.
- [17] S. Papathanassiou, N. Hatziargyriou and K. Strunz, "A Benchmark Low Voltage Microgrid Network", CI-GRE TF 6.04.02, Jan. 2005.